Published in final edited form as:

J Nucl Med. 2010 January ; 51(1): 57–65. doi:10.2967/jnumed.109.065185.

Spatial Heterogeneity of Lung Perfusion Assessed with ^{13}N PET as a Vascular Biomarker in Chronic Obstructive Pulmonary Disease

Marcos F. Vidal Melo[1], **Tilo Winkler**[1], **R. Scott Harris**[2], **Guido Musch**[1], **Reginald E. Greene**[3], **Jose G. Venegas**[1]

[1]Department of Anesthesia and Critical Care, Massachusetts General Hospital and Harvard Medical School, Boston, Massachusetts

[2]Department of Medicine (Pulmonary and Critical Care Unit), Massachusetts General Hospital and Harvard Medical School, Boston, Massachusetts

[3]Department of Radiology, Massachusetts General Hospital and Harvard Medical School, Boston, Massachusetts

Abstract

Although it is known that structural and functional changes in the pulmonary vasculature and parenchyma occur in the progress of chronic obstructive pulmonary disease (COPD), information is limited on early regional perfusion ($\dot{Q}_r$) alterations.

Methods: We studied 6 patients with mild or moderate COPD and 9 healthy subjects (6 young and 3 age-matched). The PET ^{13}NN-labeled saline injection method was used to compute images of $\dot{Q}_r$ and regional ventilation ($\dot{V}_r$). Transmission scans were used to assess regional density. We used the squared coefficient of variation to quantify $\dot{Q}_r$ heterogeneity and length-scale analysis to quantify the contribution to total perfusion heterogeneity of regions ranging from less than 12 to more than 108 mm.

Results: Perfusion distribution in COPD subjects showed larger $\dot{Q}_r$ heterogeneity, higher contribution from large length scales and lower contribution from small length scales, and larger heterogeneity of $\dot{Q}_r$ normalized by tissue density than did healthy subjects. Dorsoventral gradients of $\dot{V}_r$ were present in healthy subjects, with larger ventilation in dependent regions, whereas no gradient was present in COPD. Heterogeneity of ventilation–perfusion ratios was larger in COPD.

Conclusion: $\dot{Q}_r$ is significantly redistributed in COPD. $\dot{Q}_r$ heterogeneity in COPD patients is greater than in healthy subjects, mainly because of the contribution of large lung regions and not because of changes in tissue density or $\dot{V}_r$. The assessment of spatial heterogeneity of lung perfusion with ^{13}NN-saline PET may serve as a vascular biomarker in COPD.

For correspondence or reprints contact: Marcos F. Vidal Melo, Department of Anesthesia and Critical Care, Harvard Medical School, Massachusetts General Hospital, 55 Fruit St., Boston, MA 02114. mvidalmelo@partners.org.

Keywords

positron-emission tomography; pulmonary circulation; chronic obstructive pulmonary disease; pulmonary gas exchange; length scale analysis

Chronic obstructive pulmonary disease (COPD) produces marked changes in the distribution of alveolar gas, ventilation, and perfusion (1,2). However, there is still limited knowledge on the topographic distributions of lung perfusion and ventilation in COPD subjects, despite the significant effect of those distributions on gas exchange (3).

Changes in the pulmonary circulation have significant clinical importance in COPD. For example, pulmonary hypertension is an independent predictor of poor prognosis (4,5). The remodeling of lung tissue, represented radio-graphically by the redistribution of regional lung density (D_r) (1,6), is thought to affect the redistribution of regional lung perfusion ($\dot{Q}_r$) in COPD (7). Using PET of a single lung slice, Brudin et al. (8) observed that the ratio of $\dot{Q}_r$ to extravascular density was similar in chronic bronchitis and emphysema, implying that the loss of vascular structures parallels tissue destruction. However, vascular structural changes without tissue loss have been reported (9). Furthermore, recent studies showed vascular dysfunction such as reduction in the expression of prostacyclin synthase (10) and downregulation of nitric oxide production in pulmonary arteries (11) during COPD.

Although it has been documented that perfusion heterogeneity increases during COPD (2), it is not known whether topographic changes in perfusion are detectable early in the disease process and at what structural level (length scale) the increase in heterogeneity occurs (lobar, segmental, or subsegmental). The relevance of understanding such perfusion changes has been recently stressed by the hypothesis that early changes in perfusion could precede changes in tissue density in COPD (12). In that case, because progressively larger regions of low density are observed in the lungs of COPD subjects as disease severity increases, it could be speculated that changes in perfusion toward larger length scales would be expected during milder stages of the disease.

Early investigations with planar xenon scans showed decreased ventilation and ventilation-to-perfusion ($\dot{V}_A/\dot{Q}$) ratio in basal pulmonary regions of subjects with chronic bronchitis (13), whereas apical regions were found to be more affected in subjects with early emphysema (13). Less is known about the vertical (i.e., dorsoventral) gradient of ventilation in supine spontaneously breathing COPD subjects. This gradient is likely affected by changes in lung expansion and thoracic cage movement observed during COPD—that is, by a reduced vertical gradient of lung inflation (6) and a possibly more uniform diaphragmatic excursion along the dorsoventral axis (14). In COPD subjects, compared with healthy subjects, such factors would be expected to reduce the vertical gradient of ventilation.

We have developed methods to estimate $\dot{Q}_r$ and regional ventilation ($\dot{V}_r$) using PET, including tracer kinetics analysis to assess small-length-scale ventilation and ($\dot{V}_A/\dot{Q}$) heterogeneity within the imaging resolution unit (voxel) (15–18). In the present study, we used these techniques to quantify the topographic distributions of perfusion, ventilation, and

gas fraction in supine healthy and COPD subjects to test the following hypotheses: $\dot{Q}_r$ is topographically redistributed during COPD, with length-scale components of perfusion heterogeneity larger than those observed in healthy subjects; perfusion heterogeneity in COPD subjects is larger than that in healthy subjects, even when changes in regional lung density are accounted for; and the vertical gradient of regional ventilation is smaller in COPD than in healthy subjects.

MATERIALS AND METHODS

Subjects

The study was approved by the Institutional Review Board of the Massachusetts General Hospital. Inclusion criteria were adult volunteers of either sex (age, 18–65 y) with mild or moderate COPD at the time of recruitment, as defined by Global Initiative for Chronic Obstructive Lung Disease criteria (19). Exclusion criteria were severe COPD (forced expiratory volume in 1 s [FEV_1], <30% predicted), continuous oxygen therapy, daily oral steroids for COPD, inability to lie flat or to hold the breath for more than 20 s, PaO_2 less than 70 mm Hg, bicarbonate greater than 27 mEq/L, ischemic heart disease or heart failure (or ejection fraction < 40%), pulmonary hypertension (mean pulmonary artery pressure > 25 mm Hg), other known lung disease or exposure to agents associated with pulmonary disease (i.e., asbestos, silica), and pregnancy.

Fifteen subjects were studied: 6 young healthy subjects, 6 subjects with COPD, and 3 healthy subjects who were age-matched to the COPD subjects. COPD subjects were receiving bronchodilators (albuterol, $n = 5$, and ipratropium bromide, $n = 3$) and inhaled steroids ($n = 4$) as part of their treatment, and these were maintained on the day of the study. Subjects were free of infections or exacerbations for 1 mo before the study (no oral prednisone or antibiotics) and did not have any other known cardiac or pulmonary disease, particularly asthma.

Emphysema was assessed by an experienced radiologist using 1.25-mm sections of high-resolution CT in 5 COPD subjects, including the 3 with the lowest spirometry values. The assessment was based on identifying visibly dilated airspaces on lung windows (window width, 1,500 Hounsfield units; window level, −500 Hounsfield units) in 3 sections in each of 3 *z*-axis lung zones (apex–aortic arch, aortic arch–left atrium, and left atrium–diaphragm). Mild emphysema (involvement of less than 10% of lung area, which was limited to the upper zone) was identified in 4 of 5 subjects. Mild to moderate emphysema (involvement of 10%–20% of lung area in the upper 2 lung zones) was identified in 1 subject.

All healthy subjects were nonsmokers and nonobese and had normal pulmonary function tests. Informed consent was obtained from each subject before the study. All subjects (healthy and COPD) underwent upright spirometry, lung volume, and diffusing capacity for carbon monoxide measurements on the day of the study (Table 1).

Experimental Procedures

Imaging Protocol.—A catheter was placed in an antecubital vein for radioisotope injection. Subjects were positioned supine and with arms abducted on the scanner table. Pulse oximetry was monitored and lung volume was continuously measured by impedance plethysmography (Respitrace; Non-Invasive Monitoring Systems). After acquisition of a transmission scan, subjects were instructed to take 2 consecutive deep breaths. During the exhalation phase of the second breath, subjects were instructed to stop exhaling for 30–40 s, when mean lung volume was reached. Mean lung volume was identified during 1 min of steady breathing before the 2 deep breaths. Simultaneously with the beginning of apnea, a bolus of ^{13}NN-saline was injected intravenously, and a PET emission scan consisting of 28 frames (8 × 2.5, 16 × 5, and 4 × 30 s) was initiated (15,17,18). At the end of apnea, the subjects were instructed to resume breathing matching their baseline respiratory rate and tidal volume displayed on a screen.

PET.—We used a PC-4096 PET scanner (Scanditronix AB) that imaged 15 contiguous 6.5-mm-thick slices of the thorax, providing 3-dimensional information over a 9.7-cm-long cylinder. Subjects were positioned in the PET scanner to include the largest amount of lung volume within the imaging field. Transmission scans (10 min) were recorded using a rotating pin source of ^{68}Ge/^{68}Ga. These scans were used to correct the emission scans for energy attenuation caused by body tissues and supporting structures, demarcate the lung field, and compute D_r and gas fraction (F_{gas}). Lung density was computed by scaling the transmission scan to a range of 0 (defined as the attenuation of air) to 1 (defined as the attenuation of the heart). F_{gas} was computed as $(1 - D_r)$ and represented the fraction of the volume of a voxel occupied by gas. Emission scans were obtained using the ^{13}NN-saline bolus infusion technique described in detail previously (15,17). A sample of the infusate was collected to assess its specific activity in a well counter cross-calibrated with the PET scanner. The total administered dose per scan was 457 ± 171 MBq.

PET Image Analysis

Emission scans were reconstructed with correction for detector sensitivity and for tissue attenuation using a convolution back-projection algorithm with a Hanning filter, yielding an effective measured spatial resolution of 8.3 mm. Resulting images consisted of an interpolated matrix of 128 × 128 × 15 voxels of 4 × 4 × 6.5 mm. To reduce imaging noise, scans were low-pass-filtered to 13 × 13 mm in the image plane, and a 2-point moving average filter was applied in the *z*-axis to a final volumetric resolution of approximately 2.2 cm^3.

The lung fields were defined by thresholding the transmission scans and then manually removing regions corresponding to main bronchi and large pulmonary vessels (15). Images of $\dot{Q}_r$ were obtained by calculating the mean ^{13}NN activity per voxel measured from the plateau phase of the ^{13}NN kinetics during the apnea (17). Mean-normalized $\dot{Q}_r$ was computed as the ratio between tracer concentration in each voxel and mean tracer concentration of all voxels in the imaged lung field. Specific ventilation (s $\dot{V}_r$) was computed as previously described (17,20) from the tracer kinetics over the entire washout period, using

a 2-compartment analysis to account for intravoxel ventilation heterogeneity. An indicator of absolute $\dot{V}_r$ was calculated as the voxel-by-voxel product of regional s $\dot{V}_r$ and gas content ($\dot{V}_r = s\dot{V}_r \cdot F_{gas}$).

Mean-normalized $\dot{V}_A/\dot{Q}$ distributions were computed as previously described (17). This analysis also takes into account the presence of $\dot{V}_A/\dot{Q}$ heterogeneity underlying the voxel size. The computed $\dot{V}_A/\dot{Q}$ were grouped on a logarithmic scale into bins of equal width ranging from −3 to 2 (i.e., $\dot{V}_A/\dot{Q}$ = 0.001–100), with a bin width of 0.1. The heterogeneity of the $\dot{V}_A/\dot{Q}$ distribution was calculated as the SD over the mean ($CV_{\dot{V}/M\dot{Q}}$). In addition, an index of low and shunting $\dot{V}_A/\dot{Q}$ areas (shunt) was computed as the fraction of total perfusion reaching areas with $\dot{V}_A/\dot{Q}$ s smaller than 0.001.

For each voxel, $\dot{Q}_r$, $s\dot{V}_r$, $\dot{V}_r$, and F_{gas} were regressed versus the vertical distance from the most dependent point of the imaged lung field. Gradients, measured from the slope of the corresponding regression line, were expressed in percentage of the mean per centimeter. Negative gradients indicate a decrease of the variable from the dependent to the nondependent regions.

Perfusion-to-density ratios ($\dot{Q}_r/D_r$) were computed by voxel-by-voxel division of $\dot{Q}_r$ by the respective D_r. Squared coefficients of variation ($CV^2 = [SD/mean]^2$) were used to quantify the spatial heterogeneity of $\dot{Q}_r(CV^2_{\dot{Q}r})$, $\dot{Q}_r/D_r(CV^2_{\dot{Q}r/Dr})$, $s\dot{V}_r(CV^2_{s\dot{V}r})$, and F_{gas} $F_{gas}(CV^2_{Fgas})$ (21).

Perfusion Heterogeneity

Heterogeneity of perfusion was determined after removing the contribution of low-count statistics (imaging noise) to the total heterogeneity of ^{13}NN apnea images (15). Briefly, we identified in the time-activity curve of the PET scan all apnea frames in which pulmonary tracer activity remained virtually constant. A minimum of 3 such frames was present for each scan. To estimate the contribution of imaging noise to total heterogeneity, we time-averaged the voxel activity of all possible combinations of plateau frames and calculated the heterogeneity of each combination image (15). We then regressed the heterogeneity of each combination image versus the inverse of the time–activity product of each image (1/[activity·time]), which is proportional to the number of counts of the image. The *y*-intercept of the linear regression represents the estimated heterogeneity of perfusion after correction for the effect of low-count statistics ($CV^2_{\dot{Q}r}$). The contribution of the vertical gradient to this heterogeneity was calculated as:

$$CV^2_{\dot{Q}r\ grad} = r^2_{\dot{Q}r\ grad} \times CV^2_{\dot{Q}r}, \quad \text{Eq. 1}$$

where $r^2_{\dot{Q}r\ grad}$ is the coefficient of determination of the regression yielding the vertical gradient. The residual heterogeneity (i.e., the heterogeneity of perfusion not explained by the vertical gradient) is then:

$$CV^2_{\dot{Q}r\ res} = CV^2_{\dot{Q}r} - CV^2_{\dot{Q}r\ grad}. \quad \text{Eq. 2}$$

Length-Scale Analysis

The contribution of different length scales to perfusion heterogeneity was assessed by computing $CV^2_{\dot{Q}r\ res}$ over a range of spatial resolutions. This calculation was performed as follows. The ^{13}NN scans were low-pass-filtered at 12, 36, 60, 84, and 108 mm, with correction for edge effects (22), and $CV^2_{\dot{Q}r\ res}$ was computed for each filter size. The absolute contribution of the specific length-scale range to $CV^2_{\dot{Q}r\ res}$ ($CV^2_{\dot{Q}r}$ LS1-LS2, where LS1–LS2 is the length-scale range) was calculated as the difference in $CV^2_{\dot{Q}r\ res}$ between the 2 successive filter sizes:

$$CV^2_{\dot{Q}r}\ LS1 - LS2 = CV^2_{\dot{Q}r\ res}\ LS1 - CV^2_{\dot{Q}r\ res}\ LS2, \quad \text{Eq. 3}$$

where $CV^2_{\dot{Q}r\ res}$ LS1 and $CV^2_{\dot{Q}r\ res}$ LS2 are the $CV^2_{\dot{Q}r\ res}$ computed for the images low-pass-filtered at LS1 and LS2.

The relative contribution of length scales was computed by dividing the absolute contribution of the specific length-scale ranges by $CV^2_{\dot{Q}r\ res}$ at 12-mm filter size. Similarly, the contribution of different length scales to the heterogeneity of F_{gas} was assessed by low-pass filtering the transmission scan at 12, 36, 60, 84, and 108 mm and computing corresponding CV^2_{Fgas}:

$$CV^2_{Fgas}\ LS1 - LS2 = CV^2_{Fgas}\ LS1 - CV^2_{\dot{Q}r\ res}\ LS2, \quad \text{Eq. 4}$$

where CV^2_{Fgas} LS1-LS2 is the contribution of the length-scale range LS1–LS2 to F_{gas} heterogeneity, and CV^2_{Fgas} LS1 and CV^2_{Fgas} LS2 are the CV^2_{Fgas} computed for the transmission scans low-pass-filtered at LS1 and LS2.

Statistical Analysis

One-way ANOVA was used for comparisons between the groups of young healthy subjects, age-matched healthy subjects, and COPD subjects. When a probability value under 0.05 was found for the overall comparison, specific comparisons between individual groups were performed. Adjustment for multiple comparisons was performed using the Tukey–Kramer

method (SAS for Windows, version 9.1.3; SAS Institute Inc.). Statistical significance was set at a value of P less than 0.05. Values are presented as mean ± SD.

RESULTS

General characteristics of the subjects are presented in Table 1. COPD subjects showed lower FEV_1, higher lung volumes, and lower CO diffusing capacity than did healthy controls.

Regional F_{gas}

Mean F_{gas} was similar in young and age-matched healthy subjects and not significantly higher in COPD patients (Fig. 1A; Table 2). No significant difference was observed in the overall spatial heterogeneity of F_{gas} (CV^2_{Fgas}) between healthy controls and COPD subjects (Table 2). The length-scale components of CV^2_{Fgas} were also similar among the groups (Fig. 2A). Dorsoventral gradients of F_{gas} in the healthy subjects were positive, indicating greater F_{gas} in nondependent than in dependent lung regions (Table 2). In contrast, those gradients were not significantly different from zero in COPD subjects. Consistent with this, the component of CV^2_{Fgas} attributable to the vertical dependence of F_{gas} was negligible in COPD.

Regional Ventilation and Ventilation-Perfusion Distributions

$s\dot{V}_r$ was on average lower and more heterogeneous in COPD than in healthy subjects (Table 2). In COPD subjects, PET images at the end of the washout showed regions of tracer retention dispersed throughout the lungs. In healthy subjects, the vertical gradient of $s\dot{V}_r$ was negative (Table 2), indicating that $s\dot{V}_r$ was larger in dorsal than in ventral regions. In contrast, for COPD subjects, the vertical gradients of both $s\dot{V}_r$ and $\dot{V}_r$ were not different from 0. The Spearman rank correlation coefficient between the vertical gradients of $s\dot{V}_r$ and F_{gas} for all the subjects studied was 0.84 ($P < 0.001$).

$\dot{V}_A/\dot{Q}$ distributions were unimodal in healthy and COPD subjects. The distribution of $\dot{V}_A/\dot{Q}$ ratios in COPD subjects was significantly broader than in young healthy subjects and also tended to be broader than in age-matched healthy subjects (Table 3). Furthermore, the component of the $\dot{V}_A/\dot{Q}$ distribution corresponding to low $\dot{V}_A/\dot{Q}$ and shunting regions was greater in COPD subjects than in both healthy groups (Table 3).

Regional Perfusion Distribution

Vertical dependence of perfusion was observed for all groups, with negative slopes of the vertical gradients, indicating higher perfusion in the dorsal than in the ventral regions (Table 3). Vertical $\dot{Q}_r$ gradients tended to be steeper, although not significantly so, in young healthy subjects than in COPD and age-matched healthy subjects. Heterogeneity of $\dot{Q}_r$ was similar in young and age-matched healthy subjects but significantly larger in the COPD subjects (Table 3; Fig. 1B).

Perfusion heterogeneity was similar between age-matched and young healthy subjects across all length-scale components (Fig. 2B). In contrast, in COPD subjects we found a larger $\dot{Q}_r$ heterogeneity than in healthy subjects at all length scales (Figs. 1B and 2B). Remarkably, for length scales between 60 and 108 mm there was no overlap between $CV_{\dot{Q}r}^2$ of healthy and COPD subjects (i.e., the $\dot{Q}_r$ heterogeneity measurements at these length scales completely separated the COPD from the healthy groups). COPD subjects showed a greater relative contribution from large (>60 mm) than from small (12–36 mm) length scales to total $\dot{Q}_r$ heterogeneity (Fig. 3). Large length-scale changes in $\dot{Q}_r$ were not consistently spatially matched to those in s $\dot{V}_r$ (Fig. 4).

Distributions of regional $\dot{Q}_r/D_r$ were unimodal for all groups but significantly broader in COPD than in healthy subjects (Fig. 5). $CV^2_{\dot{Q}r/Dr}$ was 2 to 3 times larger in COPD than in either age-matched or young healthy subjects (Table 3); that is, the increased heterogeneity of perfusion persisted when $\dot{Q}_r$ was normalized by regional tissue density.

DISCUSSION

The following are the main findings of this study. First, $\dot{Q}_r$ distribution in subjects with COPD is markedly different from that in healthy subjects. Absolute perfusion heterogeneity is higher at all length scales in subjects with COPD. However, that increase is topographically uneven, with a greater relative contribution of larger length scales to perfusion heterogeneity in COPD subjects and of smaller length scales in healthy controls. Second, the difference in perfusion heterogeneity between COPD and healthy subjects cannot be explained exclusively by changes in regional density, because such a difference persists after normalization by tissue density. Finally, s $\dot{V}_r$ is distributed more heterogeneously but with a smaller dorsoventral gradient in COPD than in healthy subjects.

Regional F_{gas}

There was no difference between groups in F_{gas} heterogeneity or length-scale components, except for the higher component due to the vertical gradient of F_{gas} in healthy subjects. MRI studies in advanced COPD found an increased heterogeneity in the apparent diffusion coefficient, an index of the size and morphology of the distal airways (23). Our finding is, thus, consistent with mild COPD, with changes in the length-scale distribution of F_{gas} not yet marked enough to deviate from those in healthy subjects.

We found no systematic vertical gradient of F_{gas} in COPD, in contrast to significant gradients in healthy subjects. This finding agrees with CT results and is likely due to reduced elastic recoil and airway obstruction causing gas trapping in dependent zones (1,6).

Perfusion Distribution

Vertical gradients of perfusion with increased blood flow in dependent regions were more pronounced in young healthy subjects than in COPD and age-matched healthy subjects. This

result in healthy subjects is consistent with studies using MRI (24), SPECT (25), and PET (15).

Perfusion was more heterogeneously distributed in COPD than in healthy subjects, in line with known pathologic changes in the pulmonary circulation during COPD (26,27). MRI studies of subjects with severe COPD showed increased perfusion heterogeneity (28) and revealed that most perfusion defects were heterogeneous and located in areas of low attenuation on CT (29). Our results advance those findings by showing that increased $\dot{Q}_r$ heterogeneity is also present and detectable with PET in mild COPD, even before significant changes in tissue density.

Moreover, the topographic study of $\dot{Q}_r$ heterogeneity with length-scale analysis evidenced several distinctions between COPD and healthy subjects, independent of age. Absolute $\dot{Q}_r$ heterogeneity was increased at all length scales in the lungs of COPD subjects, compared with those of healthy subjects. This increase was particularly evident at length scales between 60 and 108 mm, in which there was no overlap between those groups (Supplemental Fig. 1; supplemental materials are available online only at http://jnm.snmjournals.org). When the relative contribution of length scales to $\dot{Q}_r$ heterogeneity was calculated, segmental to lobar-sized regions contributed significantly more to global perfusion heterogeneity in COPD than in healthy subjects. In contrast, the contribution of regions in the 12-to 36-mm range to global perfusion heterogeneity was significantly larger in healthy subjects.

Changes in the pulmonary circulation in COPD have been traditionally viewed as the result of destruction of the vascular bed and hypoxic pulmonary vasoconstriction (HPV) (5,7,26). In fact, Brudin et al. implied that the loss of vascular structures parallels tissue destruction in emphysema (8). Although this may occur in advanced COPD, it does not seem to apply in our subjects with milder disease. Indeed, if tissue loss were the only factor explaining the differences in perfusion heterogeneity, the $\dot{Q}_r/D_r$ distribution should have been similar in COPD subjects and healthy subjects. Instead, we found a significantly larger $\dot{Q}_r/D_r$ heterogeneity in COPD than in healthy subjects, implying that a significant component of perfusion redistribution in mild COPD is associated with factors unrelated to regional density. Finally, the fact that topographic changes of perfusion did not match those of ventilation (Fig. 4) and that $\dot{V}_A/\dot{Q}$ heterogeneity was higher in COPD subjects suggests that HPV was not a dominating factor in the observed redistribution of $\dot{Q}_r$.

Vascular dysfunction and remodeling would be likely mechanisms contributing to the increased $\dot{Q}_r/D_r$ heterogeneity. Recent studies indicated the direct vascular effect of tobacco smoke on the intrapulmonary vessels leading to aberrant vascular function and remodeling (5,7). Endothelial dysfunction has been documented in COPD by the altered pulmonary kinetics of ^{123}I-metaiodobenzyl-guanidine (30), loss of nitric oxide–dependent relaxation in extrapulmonary arterioles (31), reduced expression of prostacyclin synthase in pulmonary arterioles (10), increased circulating levels of endothelin (32), and increased apoptosis of

alveolar endothelial and epithelial cells (33). These factors compound with pulmonary vessel intimal thickening during mild disease that progresses to medium and adventitia thickening in moderate and severe COPD (9). Independent of the exact mechanisms, the observed heterogeneity of perfusion, before significant F_{gas} changes are present, could represent the initial inflammation and remodeling stages of the pulmonary circulation that precede pulmonary hypertension, a well-established ominous prognostic sign in COPD (4). In this case, an important implication of our findings is that the detected changes in $\dot{Q}_r$ and $\dot{Q}_r/D_r$ distribution could represent a component of vascular alterations preceding tissue destruction and potentially amenable to treatment. Longitudinal studies of subjects at risk for COPD, potentially using PET/CT techniques, will be needed to verify this hypothesis. In light of the promise of imaging biomarkers to study lung disease (34), our results suggest the potential role of the distribution of $\dot{Q}_r$ and $\dot{Q}_r/D_r$ as important biomarkers in COPD.

Why an increased contribution from large length scales to $\dot{Q}_r$ heterogeneity would derive from those vascular changes is currently unknown. Potentially, those changes could result in altered control of $\dot{Q}_r$ in large vessels or in anatomically clustered small vessels. This could occur if large or groups of small vessels became more muscularized or active in COPD (9) or if loss of vasculature or modification of regional vasoreactivity at the alveolar or small-length-scale level would produce a network effect amplifying the role of larger vessels in the regional control of perfusion, analogous to the mechanism resulting in hypoventilation clusters in patients with asthma (35). Higher perfusion heterogeneity at large length scales could also be a precursor of the patchy tissue destruction in later stages of COPD. In fact, the decrease of perfusion to inflamed areas has been hypothesized as a cause of parenchymal destruction in COPD (12). Additionally, if tissue properties change with perfusion redistribution, local mechanical forces may be amplified and facilitate stress failure and tissue destruction (36).

Regional Ventilation

COPD subjects presented lower mean s $\dot{V}_r$ and larger ventilation heterogeneity than healthy subjects, in accordance with previous studies (2,13). The negative ventilation gradients we found in healthy subjects are consistent with previous studies (37) and with larger excursion of the dependent portion of the diaphragm in these subjects (38). Such results also suggest that the changes in the vertical gradient of s $\dot{V}_r$ are more likely due to the disease process than to aging. Changes in chest wall expansion and diaphragmatic motion could also contribute to changes in regional ventilation, despite significant controversy on this issue (39,40). Our findings that the vertical gradient of ventilation is smaller in COPD whereas total ventilation heterogeneity is higher also suggest that heterogeneity at the isogravitational level is higher in COPD than in healthy subjects.

Ventilation–Perfusion in Supine COPD

We found increased $\dot{V}_A/\dot{Q}$ heterogeneity with broad unimodal $\dot{V}_A/\dot{Q}$ distributions, consistent with the moderate degree of disease in our subjects (2). The finding that $CV^2_{\dot{Q}r}$ and $CV^2_{s\dot{V}r}$

were larger in COPD than in healthy subjects implies that the increased $\dot{V}_A/\dot{Q}$ mismatch was due to maldistributions of both ventilation and perfusion. The increased $\dot{V}_A/\dot{Q}$ heterogeneity also implies that, even if HPV were present, the spatial $\dot{Q}_r$ heterogeneity in COPD subjects did not completely match s $\dot{V}_r$ heterogeneity.

Methodologic Aspects and Limitations

Limitations of the used techniques have been discussed in detail (15,17). Although PET scans have lower resolution than do CT scans, their in-plane resolution of 6 mm is largely sufficient to quantify functional imaging parameters such as F_{gas} and vertical gradients (15). The resolution of the PET scans defines the lower boundary for the quantification of F_{gas} and $\dot{Q}_r$ heterogeneity, which we set at 2 times the in-plane resolution (≥12 mm). Registration errors may occur at the voxel level between images acquired during breath-hold ($\dot{Q}_r$) and during breathing (s $\dot{V}_r$, D_r, F_{gas}) and affect estimates of small-length-scale heterogeneity. However, the observed separation between COPD and healthy groups at larger length scales is not likely to be affected by such errors. Because the same imaging methods were used in each subject, differences among groups cannot be explained by misregistration errors, which would be equivalent in all groups. Furthermore, we demonstrated previously (17) a high correlation between direct measurements of arterial blood gas and blood gas estimates derived from our images of $\dot{Q}_r$ and s $\dot{V}_r$, even for significantly heterogeneous ($\dot{V}_A/\dot{Q}$) distributions. This suggests that motion artifacts were not large enough to compromise the quantitative value of the techniques in healthy and disease conditions.

Sex was distributed unevenly in the groups. There is no evidence in the literature or in our data that sex affects the topographic distribution of perfusion, ventilation, or F_{gas}. Consequently, it is unlikely that sex imbalance would explain our results.

CONCLUSION

We found a significant topographic redistribution of $\dot{Q}_r$ in subjects with COPD, despite there being only mild emphysematous changes in 5 of 6 by CT. The larger perfusion heterogeneity could not be explained exclusively by changes in regional tissue density. The observed changes in $\dot{Q}_r$, detected noninvasively with PET, may warrant further investigation as an early biomarker of the pulmonary vascular involvement in COPD.

Supplementary Material

Refer to Web version on PubMed Central for supplementary material.

ACKNOWLEDGMENTS

We thank Steven B. Weise, PET Imaging Laboratory, Massachusetts General Hospital, for his expert support in the acquisition of images. This study was funded by NIH grants R01-HL-086827 and HL-068011.

REFERENCES

1. Goddard PR, Nicholson EM, Laszlo G, Watt I. Computed tomography in pulmonary emphysema. Clin Radiol. 1982;33:379–387. [PubMed: 7083738]
2. Wagner PD, Dantzker DR, Dueck R, Clausen JL, West JB. Ventilation-perfusion inequality in chronic obstructive pulmonary disease. J Clin Invest. 1977;59:203–216. [PubMed: 833271]
3. West JB. Distribution of mechanical stress in the lung, a possible factor in localisation of pulmonary disease. Lancet. 1971;1:839–841. [PubMed: 4102531]
4. Weitzenblum E, Hirth C, Ducolone A, Mirhom R, Rasaholinjanahary J, Ehrhart M. Prognostic value of pulmonary artery pressure in chronic obstructive pulmonary disease. Thorax. 1981;36:752–758. [PubMed: 7330793]
5. Wright JL, Levy RD, Churg A. Pulmonary hypertension in chronic obstructive pulmonary disease: current theories of pathogenesis and their implications for treatment. Thorax. 2005;60:605–609. [PubMed: 15994270]
6. Millar AB, Denison DM. Vertical gradients of lung density in supine subjects with fibrosing alveolitis or pulmonary emphysema. Thorax. 1990;45:602–605. [PubMed: 2402722]
7. Hopkins N, McLoughlin P. The structural basis of pulmonary hypertension in chronic lung disease: remodelling, rarefaction or angiogenesis? J Anat. 2002;201:335–348. [PubMed: 12430958]
8. Brudin LH, Rhodes CG, Valind SO, Buckingham PD, Jones T, Hughes JM. Regional structure-function correlations in chronic obstructive lung disease measured with positron emission tomography. Thorax. 1992;47:914–921. [PubMed: 1465748]
9. Magee F, Wright JL, Wiggs BR, Pare PD, Hogg JC. Pulmonary vascular structure and function in chronic obstructive pulmonary disease. Thorax. 1988;43:183–189. [PubMed: 3406902]
10. Nana-Sinkam SP, Lee JD, Stearman R, et al. Prostacyclin synthase in smoking-related lung disease [abstract]. Proc Am Thorac Soc. 2006;3:517.
11. Sin DD, Man SF. Is systemic inflammation responsible for pulmonary hypertension in COPD? Chest. 2006;130:310–312. [PubMed: 16899824]
12. Hoffman EA, Simon BA, McLennan G. State of the art: a structural and functional assessment of the lung via multidetector-row computed tomography—phenotyping chronic obstructive pulmonary disease. Proc Am Thorac Soc. 2006;3:519–532. [PubMed: 16921136]
13. Anthonisen NR, Bass H, Oriol A, Place RE, Bates DV. Regional lung function in patients with chronic bronchitis. Clin Sci. 1968;35:495–511. [PubMed: 5705805]
14. Butler C Diaphragmatic changes in emphysema. Am Rev Respir Dis. 1976;114:155–159. [PubMed: 937832]
15. Musch G, Layfield JD, Harris RS, et al. Topographical distribution of pulmonary perfusion and ventilation, assessed by PET in supine and prone humans. J Appl Physiol. 2002;93:1841–1851. [PubMed: 12381773]
16. Vidal Melo MF, Harris RS, Layfield D, Musch G, Venegas JG. Changes in regional ventilation after autologous blood clot pulmonary embolism. Anesthesiology. 2002;97:671–681. [PubMed: 12218535]
17. Vidal Melo MF, Layfield D, Harris RS, et al. Quantification of regional ventilation-perfusion ratios with PET. J Nucl Med. 2003;44:1982–1991. [PubMed: 14660725]
18. Harris RS, Winkler T, Tgavalekos N, et al. Regional pulmonary perfusion, inflation, and ventilation defects in bronchoconstricted patients with asthma. Am J Respir Crit Care Med. 2006;174:245–253. [PubMed: 16690973]
19. Pauwels RA, Buist AS, Calverley PM, Jenkins CR, Hurd SS, GOLD Scientific Committee. Global strategy for the diagnosis, management, and prevention of chronic obstructive pulmonary disease. NHLBI/WHO global initiative for chronic obstructive lung disease (GOLD) workshop summary. Am J Respir Crit Care Med. 2001;163:1256–1276. [PubMed: 11316667]
20. Venegas JG, Schroeder T, Harris S, Winkler RT, Melo MF. The distribution of ventilation during bronchoconstriction is patchy and bimodal: a PET imaging study. Respir Physiol Neurobiol. 2005;148:57–64. [PubMed: 15994134]

21. Treppo S, Mijailovich SM, Venegas JG. Contributions of pulmonary perfusion and ventilation to heterogeneity in measured by PET. J Appl Physiol. 1997;82:1163–1176. [PubMed: 9104853]
22. Venegas JG, Galletti GG. Low-pass filtering, a new method of fractal analysis: application to PET images of pulmonary blood flow. J Appl Physiol. 2000;88: 1365–1373. [PubMed: 10749831]
23. Salerno M, de Lange EE, Altes TA, Truwit JD, Brookeman JR, Mugler JP III. Emphysema: hyperpolarized helium 3 diffusion MR imaging of the lungs compared with spirometric indexes—initial experience. Radiology. 2002;222:252–260. [PubMed: 11756734]
24. Stock KW, Chen Q, Levin D, Hatabu H, Edelman RR. Demonstration of gravity-dependent lung perfusion with contrast-enhanced magnetic resonance imaging. J Magn Reson Imaging. 1999;9:557–561. [PubMed: 10232514]
25. Orphanidou D, Hughes JM, Myers MJ, Al-Suhali AR, Henderson B. Tomography of regional ventilation and perfusion using krypton 81m in normal subjects and asthmatic patients. Thorax. 1986;41:542–551. [PubMed: 3491441]
26. Liebow AA. Pulmonary emphysema with special reference to vascular changes. Am Rev Respir Dis. 1959;80:67–93. [PubMed: 13670406]
27. Reid JA, Heard BE. The capillary network of normal and emphysematous human lungs studied by injections of Indian ink. Thorax. 1963;18:201–212. [PubMed: 14064613]
28. Amundsen T, Torheim G, Waage A, Bjermer L, Steen PA, Haraldseth O. Perfusion magnetic resonance imaging of the lung: characterization of pneumonia and chronic obstructive pulmonary disease—a feasibility study. J Magn Reson Imaging. 2000;12:224–231. [PubMed: 10931584]
29. Ogasawara N, Suga K, Zaki M, Okada M, Kawakami Y, Matsunaga N. Assessment of lung perfusion impairment in patients with pulmonary artery-occlusive and chronic obstructive pulmonary diseases with noncontrast electrocardiogram-gated fast-spin-echo perfusion MR imaging. J Magn Reson Imaging. 2004;20:601–611. [PubMed: 15390150]
30. Arao T, Takabatake N, Sata M, et al. In vivo evidence of endothelial injury in chronic obstructive pulmonary disease by lung scintigraphic assessment of ^{123}I-metaiodobenzylguanidine. J Nucl Med. 2003;44:1747–1754. [PubMed: 14602855]
31. Peinado VI, Barbera JA, Ramirez J, et al. Endothelial dysfunction in pulmonary arteries of patients with mild COPD. Am J Physiol. 1998;274:L908–L913. [PubMed: 9609729]
32. Roland M, Bhowmik A, Sapsford RJ, et al. Sputum and plasma endothelin-1 levels in exacerbations of chronic obstructive pulmonary disease. Thorax. 2001;56:30–35. [PubMed: 11120901]
33. Kasahara Y, Tuder RM, Cool CD, Lynch DA, Flores SC, Voelkel NF. Endothelial cell death and decreased expression of vascular endothelial growth factor and vascular endothelial growth factor receptor 2 in emphysema. Am J Respir Crit Care Med. 2001;163:737–744. [PubMed: 11254533]
34. Schuster DP. The opportunities and challenges of developing imaging biomarkers to study lung function and disease. Am J Respir Crit Care Med. 2007;176:224–230. [PubMed: 17478617]
35. Venegas JG, Winkler T, Musch G, et al. Self-organized patchiness in asthma as a prelude to catastrophic shifts. Nature. 2005;434:777–782. [PubMed: 15772676]
36. Mishima M, Hirai T, Itoh H, et al. Complexity of terminal airspace geometry assessed by lung computed tomography in normal subjects and patients with chronic obstructive pulmonary disease. Proc Natl Acad Sci USA. 1999;96:8829–8834. [PubMed: 10430855]
37. Bryan AC, Milic-Emili J, Pengelly D. Effect of gravity on the distribution of pulmonary ventilation. J Appl Physiol. 1966;21:778–784. [PubMed: 5912747]
38. Froese AB, Bryan AC. Effects of anesthesia and paralysis on diaphragmatic mechanics in man. Anesthesiology. 1974;41:242–255. [PubMed: 4604401]
39. Suga K, Tsukuda T, Awaya H, Matsunaga N, Sugi K, Esato K. Interactions of regional respiratory mechanics and pulmonary ventilatory impairment in pulmonary emphysema: assessment with dynamic MRI and xenon-133 single-photon emission CT. Chest. 2000;117:1646–1655. [PubMed: 10858397]
40. Kleinman BS, Frey K, VanDrunen M, et al. Motion of the diaphragm in patients with chronic obstructive pulmonary disease while spontaneously breathing versus during positive pressure breathing after anesthesia and neuromuscular blockade. Anesthesiology. 2002;97:298–305. [PubMed: 12151916]

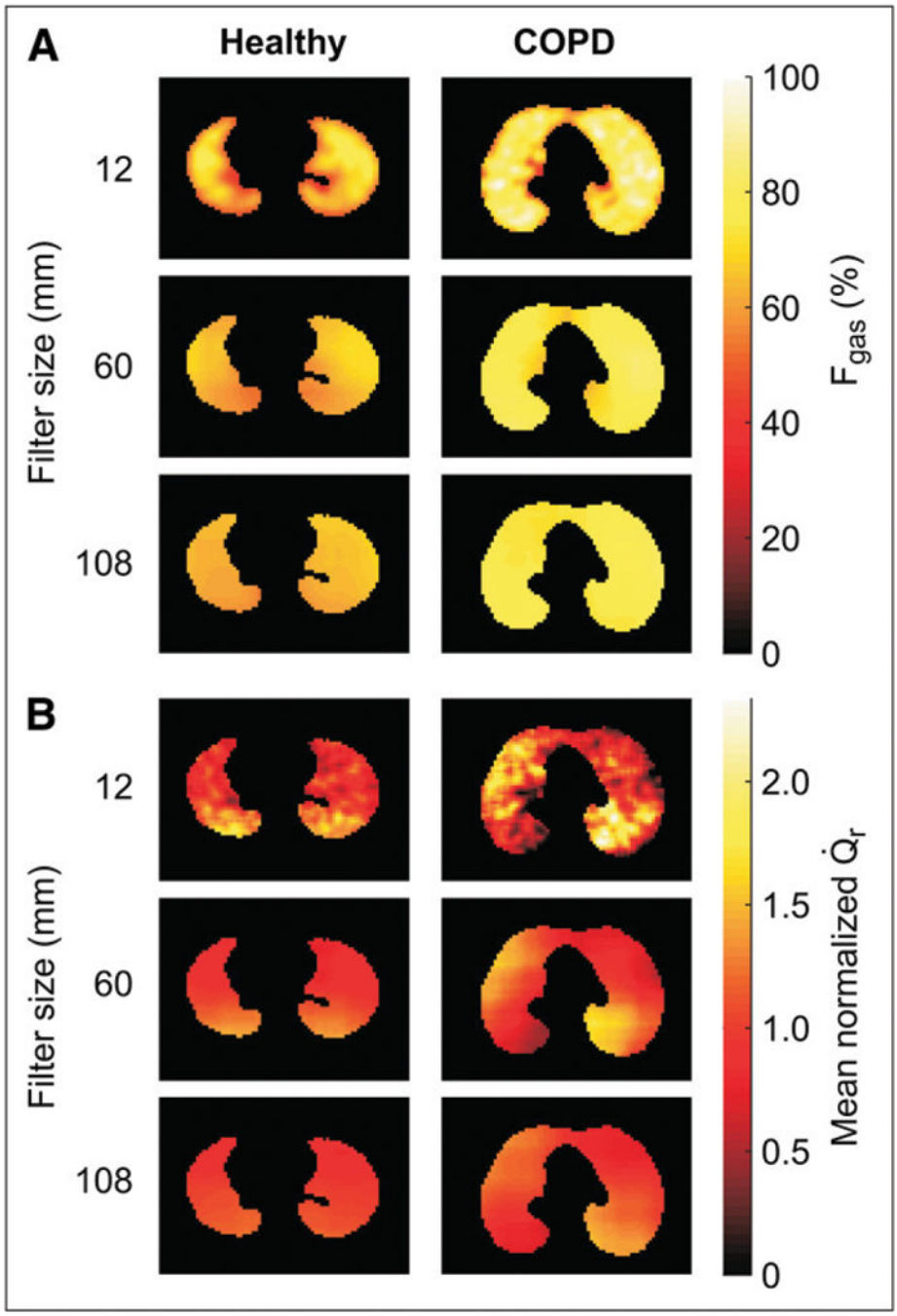

FIGURE 1.

Representative PET images of regional F_{gas} (A) and mean normalized perfusion ($\dot{Q}_r$) (B) in supine young healthy and COPD subjects for different topographic filter sizes. Images are transverse tomographic sections, with color scale representing either F_{gas} (A) or ^{13}NN activity (B). Left side in image corresponds to left lung. Heterogeneity is present in $\dot{Q}_r$ but not F_{gas} for COPD subjects at larger filter sizes, indicating large length-scale heterogeneity.

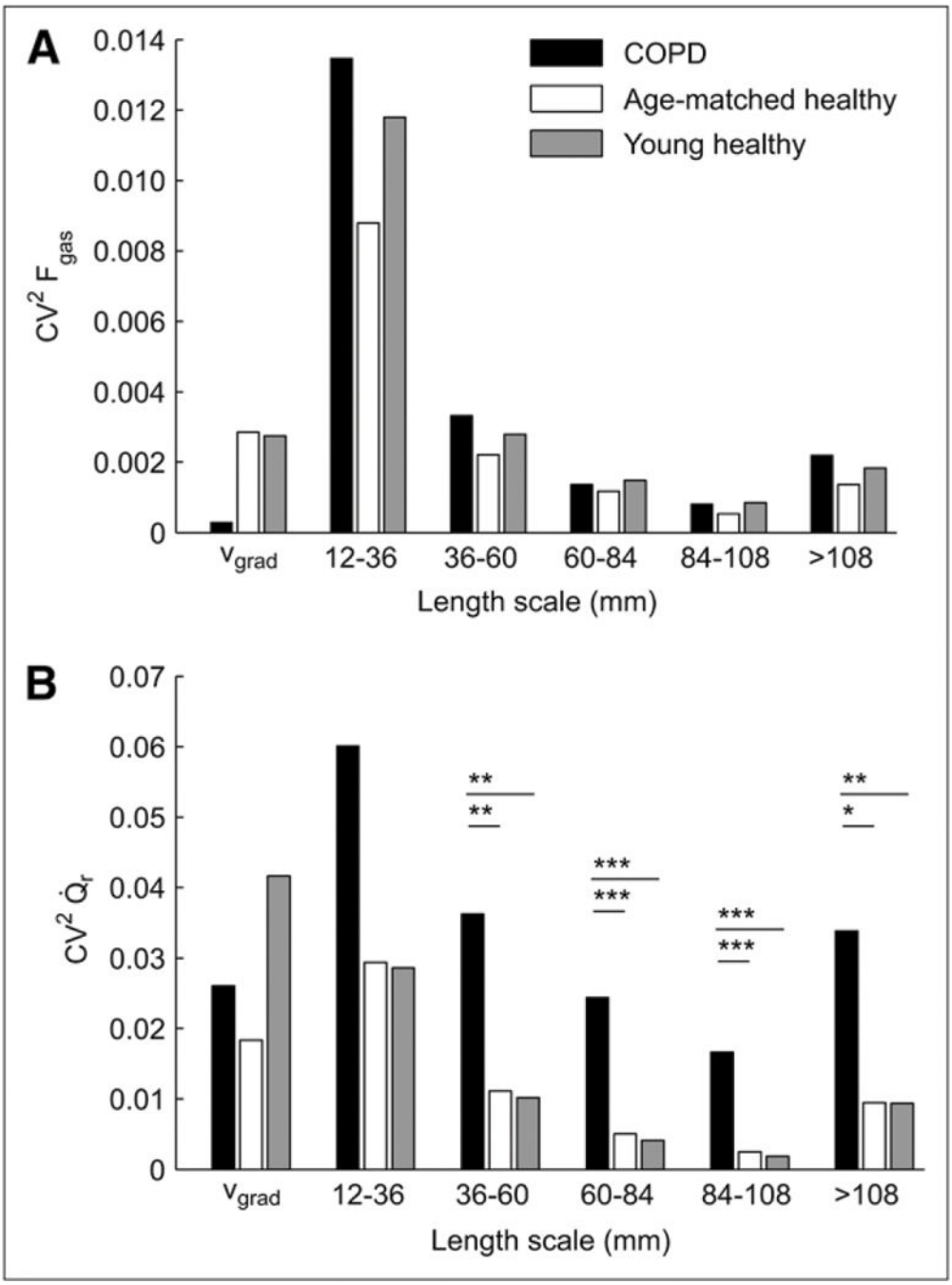

FIGURE 2.

Squared coefficient of variation (CV^2) of regional F_{gas} (A) and mean normalized perfusion ($\dot{Q}_r$) (B) pertaining to different length-scale ranges and vertical gradient (v_{grad}) in 3 groups studied: young healthy subjects ($n = 6$), age-matched healthy subjects ($n = 3$), and COPD subjects ($n = 6$). CV^2_{Fgas} was similar among all groups at each length scale. In contrast, $CV^2_{\dot{Q}r}$ heterogeneity was larger in COPD subjects than in healthy subjects for all length

scales. $CV^2_{\dot{Q}r}$ was similar at each length scale for groups of healthy subjects. *0.05 < P < 0.10. ** P < 0.05. *** P < 0.005.

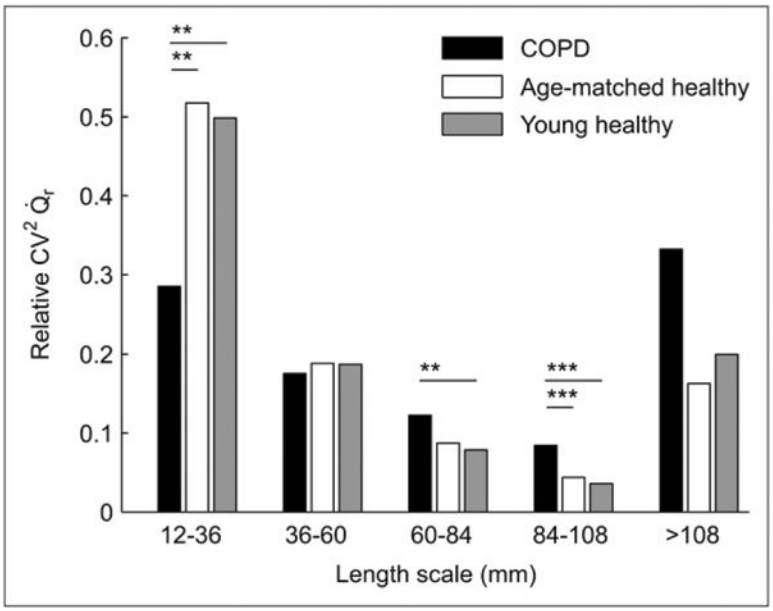

FIGURE 3.

Percentage contribution of length-scale ranges to perfusion heterogeneity (relative $CV^2_{\dot{Q}r}$) in 3 groups studied: young healthy subjects ($n = 6$), age-matched healthy subjects ($n = 3$), and COPD subjects ($n = 6$). Contribution of lower length-scale heterogeneity is greater in both normal groups, in contrast to greater contribution of large length-scale heterogeneity in COPD. $^{**}P < 0.05$. $^{***}P < 0.005$.

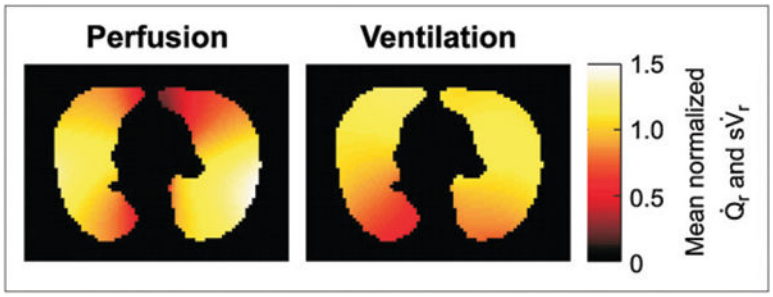

FIGURE 4.

PET image of mean normalized $\dot{Q}_r$ and $s\dot{V}_r$ filtered to length scales greater than 108 mm in COPD patient. Large length-scale heterogeneity is present in both images, but there is no full topographic matching between them.

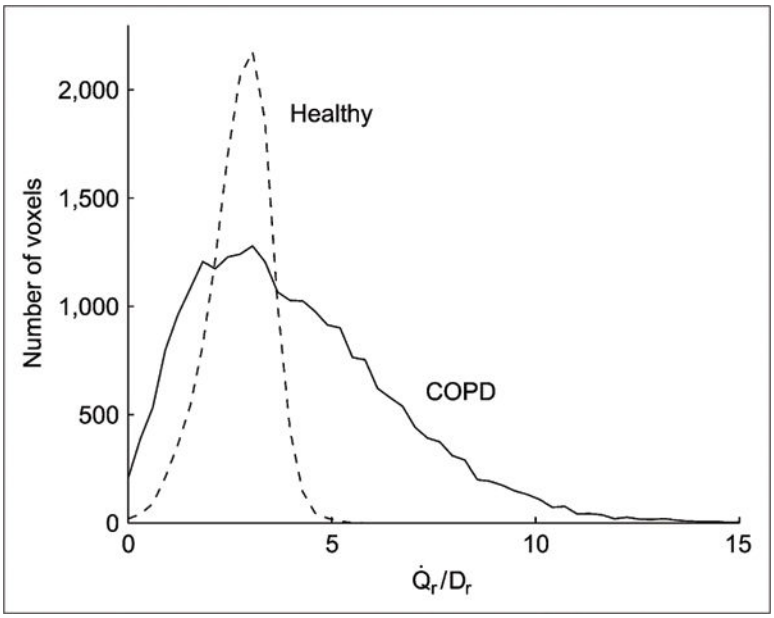

FIGURE 5.

Histograms of mean normalized $\dot{Q}_r/D_r$ ratios for whole imaged lung field in typical young healthy subject and COPD patient. Larger heterogeneity of $\dot{Q}_r/D_r$ ratio exists in COPD patient.

TABLE 1.

Demographic and Pulmonary Function Data

Parameter	Young healthy	Age-matched healthy	COPD
Age (y)	22 ± 2	58 ± 5	60 ± 6
Sex (F/M)	4/2	2/1	1/5
FEV_1 (% predicted)	97 ± 12	95 ± 15	57 ± 13[*,†]
RV/TLC (% predicted)	99 ± 6	104 ± 18	131 ± 23[‡,§]
DL_{CO} (% predicted)	102 ± 9	93 ± 12	68 ± 25[‡,‖]

[*] $P < 0.0005$ COPD vs. young healthy subjects.

[†] $P < 0.005$ COPD vs. age-matched healthy subjects.

[‡] $P < 0.05$ COPD vs. young healthy subjects.

[§] $P < 0.05$ COPD vs. age-matched healthy subjects.

[‖] $0.05 < P < 0.10$ COPD vs. age-matched healthy subjects.

Values are mean ± SD.

RV = residual volume; TLC = total lung capacity; DL_{CO} = diffusing capacity for carbon monoxide.

TABLE 2.

Regional F_{gas} and Ventilation Distributions

Parameter	Young healthy	Age-matched healthy	COPD
F_{gas} (%)	64 ± 5	68 ± 5	72 ± 7
$Fgas_{grad}$ (10^{-2} cm^{-1})	1.6 ± 1.0	1.8 ± 0.2	0.5 ± 0.4 *,†
CV^2_{Fgas}	0.022 ± 0.011	0.018 ± 0.002	0.022 ± 0.008
$s\dot{V}_r$ (10^{-3} s^{-1})	0.090 ± 0.060	0.082 ± 0.023	0.043 ± 0.014 *,†
$s\dot{V}_{r\ grad}$ (10^{-3} s^{-1} cm^{-1})	−1.2 ± 0.6	−1.3 ± 0.4	0.0 ± 0.4 ‡,§
$\dot{V}_{r\ grad}$ ($10^{-4}$$Cm^{-1}$)	−5.1 ± 2.2	−6.9 ± 2.5	0.3 ± 2.7 *,‖
$CV^2_{s\dot{V}_r}$	0.151 ± 0.043	0.206 ± 0.064	0.401 ± 0.103 §,¶

*$P < 0.05$ COPD vs. young healthy subjects.

†$0.05 < P < 0.10$ COPD vs. age-matched healthy subjects.

‡$P < 0.005$ COPD vs. young healthy subjects.

§$P < 0.01$ COPD vs. age-matched healthy subjects.

‖$P < 0.005$ COPD vs. age-matched healthy subjects.

¶$P < 0.0005$ COPD vs. young healthy subjects.

Values are mean ± SD.

$Fgas_{grad}$ = vertical gradient of F_{gas}; CV^2_{Fgas} = squared coefficient of variation of F_{gas}; $s\dot{V}_{r\ grad}$ = vertical gradient of specific ventilation; $\dot{V}_{r\ grad}$ = vertical gradient of ventilation; $CV^2_{s\dot{V}_r}$ = squared coefficient of variation of specific ventilation.

TABLE 3.

$\dot{Q}_r$, $\dot{Q}_r/D_r$, and Ventilation–Perfusion Distributions

Parameter	Young healthy	Age-matched healthy	COPD
$\dot{Q}_{r\ grad}$ (10^{-2} cm^{-1})	−5.4 ± 2.7	−2.4 ± 2.7	−2.7 ± 1.9
$CV^2_{\dot{Q}r}$	0.097 ± 0.038	0.077 ± 0.040	0.225 ± 0.057 *,†
$CV^2_{\dot{Q}r/Dr}$	0.116 ± 0.045	0.161 ± 0.041	0.333 ± 0.132 *,‡
$CV_{\dot{V}A/\dot{Q}}$	0.13 ± 0.01	0.17 ± 0.06	0.25 ± 0.07 *,‡
Low $\dot{V}_A/\dot{Q}$ and shunt (%)	1.8 ± 0.6	1.3 ± 0.2	9.8 ± 6.7 §,‖

*$P < 0.005$ COPD vs. young healthy subjects.

†$P < 0.005$ COPD vs. age-matched healthy subjects.

‡$0.05 < P < 0.10$ COPD vs. age-matched healthy subjects.

§$P < 0.05$ COPD vs. young healthy subjects.

‖$P < 0.05$ COPD vs. age-matched healthy subjects.

Values are mean ± SD.

$\dot{Q}_{r\ grad}$ = vertical gradient of regional perfusion; $CV^2_{\dot{Q}r}$ = total squared coefficient of variation of regional perfusion (noise corrected); $CV^2_{\dot{Q}r/Dr}$ = squared coefficient of variation of regional $\dot{Q}_r/D_r$ ratio; $CV_{\dot{V}A/\dot{Q}}$ = coefficient of variation of ventilation–perfusion ratios.